Comparative Analysis of Two Different Amide-to-Ester Bond Mutations in the β-Sheet of 4-Oxalocrotonate Tautomerase†

Peter Silinski and Michael C. Fitzgerald*

Department of Chemistry, Duke University, Durham, North Carolina 27708-0346

Received December 11, 2002; Revised Manuscript Received April 3, 2003

ABSTRACT: Here we describe the total chemical synthesis and biophysical characterization of two backbone-modified, ester bond-containing analogues of the homohexameric enzyme 4-oxalocrotonate tautomerase (4OT). The amide-to-ester bond mutations in the two analogues in this study, (OI2)4OT and (OI7)4OT, were designed to effectively delete specific backbone−backbone hydrogen bonds in the β-sheet region of the native 4OT hexamer. The (OI2)4OT and (OI7)4OT analogues each contained one ester bond per monomer that effectively deleted 12 backbone−backbone hydrogen bonds per hexamer. The structural properties of each analogue were characterized by size-exclusion chromatography (SEC), far-UV CD spectroscopy, and catalytic activity measurements, and they were found to be very similar to the structural properties of the wild-type enzyme. The results of equilibrium unfolding studies revealed that the (OI2)4OT and (OI7)4OT analogues were stabilized by 47.7 ± 2.5 and 45.0 ± 2.5 kcal/mol, respectively, under standard state conditions (1 M hexamer) as compared to a value of 69.6 ± 3.3 kcal/mol for the wild-type control. Our results suggest that the two different, but structurally similar, backbone−backbone hydrogen bonds deleted in (OI2)4OT and (OI7)4OT make nearly equivalent contributions to the thermodynamic stability of the 4OT hexamer.

The synthesis and biophysical characterization of protein analogues that contain backbone amide-to-ester bond mutations can provide important information about the role of the polypeptide backbone in protein folding reactions. Elements of the polypeptide backbone (e.g., amide groups) are involved in many of the native contacts in folded proteins. The large majority of these contacts are hydrogen bonding interactions that involve the pairing of oxygen atoms in backbone carbonyl groups with hydrogen atoms in backbone NH groups. Such backbone−backbone hydrogen bonds are found in α-helices, in β-sheets, and at protein−protein interfaces. However, despite their prevalence in protein structures, the thermodynamic and kinetic contributions of backbone−backbone hydrogen bonds to protein folding and stability are not well-understood (*1*−*5*). This is in large part due to the inherent difficulties associated with introducing backbone modifications into proteins using conventional site-directed mutagenesis experiments.

Recently, two new technologies (one relying on chemical synthesis strategies and one relying on a specialized *in vitro* translation technique) that permit modification of the peptide backbone in proteins have been developed (*6*, *7*). These approaches have been used in several studies to incorporate amide-to-ester bond mutations into the peptide backbone of proteins (*8*−*11*). The ester bond-containing protein analogues prepared in these studies have provided some details about the energetic contribution of backbone−backbone hydrogen bonds to protein stability. In one study, the contribution of individual hydrogen bonds at various positions in an α-helix to the overall stability of T4 lysozyme was determined to be in the range of 0.7−0.9 kcal/mol (*8*). In another study, individual backbone−backbone hydrogen bonds in a β-sheet were found to contribute between 1.5 and 2.5 kcal/mol to the stability of staphylococcal nuclease (*9*). Investigations into the complexation of serine proteinases and their protein inhibitors have evaluated the energetic contribution of backbone−backbone hydrogen bonds in these protein−protein interactions to be between 0.8 and 2.0 kcal/mol (*10*, *11*). Dawson and co-workers have shown that an analogue of chymotrypsin inhibitor 2 (CI2) containing four ester bonds destabilized CI2 by close to 1 kcal/mol per hydrogen bond deleted and that ester bond mutations in the hydrophobic core of GCN4 destabilized this coiled coil domain by ∼1.5 kcal/mol per hydrogen bond deleted (*12*, *31*). Interestingly, it was noted in the GCN4 study that the ester bond substitutions at different positions along the hydrophobic region of the GCN4 helices resulted in different degrees of destabilization (*31*). Recently, we have shown that backbone−backbone hydrogen bonding interactions involving a single amide bond in the 62-amino acid polypeptide chain of 4-oxalocrotonate tautomerase (4OT)[1] play an essential role in specifying the native conformation of this enzyme's native folded state (*13*). We have also used a backbone-modified analogue of the P22 Arc repressor to help assign a value of 2.5 kcal/mol to the energetic contribution of two backbone−backbone hydrogen bonds to the thermodynamic stability of a hyperstable P22 Arc repressor mutant (*14*).

Currently, there is no consensus with regard to the exact magnitude of the energetic contribution of backbone−backbone hydrogen bonds to protein folding reactions, and fundamental questions about the role of the peptide backbone

† This work was supported in part by a grant to M.C.F. from the National Institutes of Health (Grant RO1 GM61680).

* To whom correspondence should be addressed: Duke University, Durham, NC 27708-0346. Telephone: (919) 660-1547. Fax: (919) 660-1605. E-mail: michael.c.fitzgerald@ duke.edu.

10.1021/bi020700b CCC: $25.00
Published on Web 05/10/2003

in protein folding reactions remain. One question that has been difficult to address is related to the relative contributions of different backbone−backbone hydrogen bonds to protein folding and stability. That is, do different backbone−backbone hydrogen bonds in protein structures make equivalent contributions to protein stability, or do the contributions of different backbone−backbone hydrogen bonds vary depending on their specific position in a protein's structure? Unfortunately, this question is difficult to address using the thermodynamic data on the ester bond-containing proteins noted above. This is because the net destabilizing effects of the ester bond mutations in the above proteins include variable contributions from other terms in addition to hydrogen bond strength (e.g., configurational entropy, desolvation, and van der Waals terms) (*1*, *15*). More recently, a series of studies have exploited amide isotope effects to quantitate the stabilizing effects of backbone−backbone hydrogen bonds in folded proteins (*16*, *17*). One result from these studies was that the average backbone−backbone hydrogen bond in an α-helix appeared to be more stabilizing than the average backbone−backbone hydrogen bond in a *β*-sheet. However, in these studies, it was not possible to compare the relative bond strengths of specific backbone−backbone hydrogen bonds.

Here we report on the total chemical synthesis and characterization of two ester bond-containing analogues of the homohexameric enzyme 4-oxalocrotonate tautomerase (4OT). The ester bond mutations in the two 4OT analogues studied here were designed to delete specific backbone−backbone hydrogen bonds in the *β*-sheet region of 4OT's native three-dimensional structure. In one analogue, (OI2)4OT, the amide bond between Pro1 and Ile2 was replaced with an ester bond, and in the second analogue, (OI7)4OT, the amide bond between His6 and Ile7 was replaced with an ester bond. The ester bond mutations in these two analogues are located at positions in 4OT's polypeptide chain that are very near each other in the enzyme's folded three-dimensional structure. This facilitated a direct comparison of the hydrogen bond strengths of the two different backbone−backbone hydrogen bonds deleted in these analogues as differential effects from terms other than hydrogen bond strength (e.g., configurational entropy, desolvation, and van der Waals terms) were believed to be minimized. The results of our studies indicate that each analogue folded into a three-dimensional structure very similar to the folded structure of the wild-type enzyme and that the destabilizing effects of the ester bond mutation in each analogue were nearly identical.

MATERIALS AND METHODS

Materials. The *tert*-butoxycarbonyl (Boc) L-amino acids were purchased from Peptide Institute, Inc., and Novabiochem, and *tert*-Boc-Arg(tosyl) OCH_2 PAM resin was obtained from Applied Biosystems. L-2-Hydroxy-3-methylvaleric acid, *N*,*N*-diisopropylethylamaine, diisopropylcarbodiimide, and *N*-ethylmorpholine were purchased from Sigma-Aldrich. 2-(1*H*-Benzotriazol-1-yl)-1,1,3,3-tetramethyluronium hexafluorophosphate (HBTU) was obtained from Quantum Biotechnologies. Neat trifluoroacetic acid (biograde) was purchased from Halocarbon, and spectroscopic grade dimethylformamide was obtained from J. T. Baker. Anhydrous HF (UHP) was purchased from Matheson Gas. HPLC grade acetonitrile was purchased from Mallinckrodt. All other chemicals were reagent grade or better.

General Methods and Instrumentation. Analytical and preparative reversed-phase high-performance liquid chromatography (RP-HPLC) separations were performed on a Rainin instrument consisting of a Dynamax SD-200 Solvent Delivery System and a Dynamax variable-wavelength UV−visible absorbance detector. Analytical RP-HPLC was performed on a C_{18} Vydac column (0.46 cm × 15.0 cm, 300 Å) at a flow rate of 1 mL/min. Preparative RP-HPLC was performed on a C_{18} Vydac column (2.2 cm × 12.0 cm, 300 Å) at a flow rate of 10 mL/min. All RP-HPLC separations were performed using linear gradients of buffer B in buffer A (buffer A is 0.1% TFA in water, and buffer B is 90% acetonitrile in water containing 0.09% TFA). Detection for analytical and preparative separations was at 214 and 230 nm, respectively. SEC was also performed on the Dynamax system. SEC separations were carried out on a Superdex 75 HR 10/30 column (Pharmacia Biotech) at a flow rate of 1 mL/min, and the mobile phase was 20 mM sodium phosphate buffer (pH 8.5). Detection for SEC was at 214 nm.

ESI-MS spectra were obtained using a PE-Sciex API 150EX instrument. Typically, samples were diluted into 40% buffer B in buffer A, and then infused directly into the mass spectrometer at a flow rate of 10 *μ*L/min using a Harvard Syringe pump. All far-UV CD measurements were performed on a Jasco-710 spectropolarimeter. Spectra were acquired at 25 °C using a bandwidth of 0.5 nm. All UV−vis absorbance data were collected using a Hewlett-Packard 8452A diode array UV−vis spectrophotometer. CD and UV−vis absorbance spectra were acquired using ultra-micro quartz cuvettes (path length of 1.0 cm). Enzyme concentrations were determined using the Waddell method (*18*). All GuHCl concentrations were determined by refractive index measurements at 25 °C (*19*).

Peptide Synthesis and Purification Procedures. The synthetic 4OT analogues in this study were prepared by total chemical synthesis using manual solid-phase peptide synthesis (SPPS) methods and *in situ* neutralization protocols for Boc chemistry as described elsewhere (*20*, *21*). Syntheses were initiated on Boc-L-Arg(tosyl) OCH_2 PAM resin. Side chain protection was as follows: Arg(Tos), Asp(OcHex), Glu(OcHex), His(Bom), Lys(2-Cl-Z), Ser(Bzl), and Thr(Bzl) where Tos is Tosyl, OcHex is cyclohexyl, Bom is *tert*-butyloxymethyl, 2-Cl-Z is 2-chlorobenzyloxycarbonyl, and Bzl is benzyl. Side chain deprotection and cleavage of the peptide from the resin were carried out by treating the resin with anhydrous HF at 0 °C for 1 h. Following the removal of HF under reduced pressure, the crude peptide product from each synthesis was precipitated and washed with cold anhydrous diethyl ether, dissolved in a minimal amount of 70% acetonitrile containing 0.1% TFA, diluted

[1] Abbreviations: 4OT, 4-oxalocrotonate tautomerase; 2-HM, 2-hydroxymuconate; GuHCl, guanidine hydrochloride; UV-CD, ultraviolet circular dichroism; SEC, size-exclusion chromatography; RP-HPLC, reversed-phase high-performance liquid chromatography; ESI-MS, electrospray ionization mass spectrometry; F_{app}, apparent fraction of unfolded enzyme; ΔG_{H-6M}, free energy difference between the 4OT hexamer folded in buffer and the unfolded monomer denatured in GuHCl; ΔG_{H-3D}, free energy difference between the 4OT hexamer and the partially folded dimer populated in 4OT's GuHCl-induced equilibrium unfolding reaction; ΔG_{3D-6M}, free energy difference between the partially folded dimer populated in 4OT's GuHCl-induced equilibrium unfolding reaction and the unfolded monomer.

with water, frozen, and lyophilized. The desired product from each synthesis was purified by preparative RP-HPLC using a 40 to 60% linear gradient of buffer B in buffer A. Pure RP-HPLC fractions, as judged by ESI-MS analysis, were pooled, frozen, and lyophilized to a dry, white solid.

The ester bond in (OI2)4OT and the ester bond in (OI7)4OT were incorporated into the polypeptide backbones of these analogues by coupling L-2-hydroxy-3-methylvaleric acid (OI) instead of L-isoleucine at positions 2 and 7, respectively. The OI in each analogue was coupled at the appropriate position by following previously established protocols (*10*). The appropriate Boc-protected amino acid was coupled to the OI residue for 1 h according to previously reported protocols, and this coupling procedure was repeated twice to increase the coupling yield (*10*). The (OI2)4OT and (OI7)4OT analogues also each contained a methionine to norleucine mutation at position 45 in 4OT's polypeptide chain. This mutation was incorporated into our synthetic constructs to eliminate the possibility of side chain oxidation during synthesis. We have previously shown that this mutation does not significantly alter the structural or catalytic properties of the enzyme (*13*, *20*). As part of the work described here, we also synthesized this synthetic wild-type control [here termed 4OT(N)] and characterized the thermodynamic properties of its folding reaction.

Protein Folding Protocol. The pure, lyophilized product from each synthesis was folded by following a previously established protocol (*13*). Briefly, ~0.5−1.0 mg of the pure, lyophilized product from each synthesis was completely dissolved in 10−20 μL of 50 mM phosphate buffer (pH 8.5) containing 6.0 M guanidine hydrochloride (GuHCl). The resulting protein solutions were diluted at least 50-fold into 50 mM phosphate (pH 8.5), and each protein was allowed to refold for 1 h at room temperature before any insoluble material was pelleted by ultracentrifugation. In some cases, the analogues were refolded in a 50 mM phosphate buffer containing 0.5 M NaCl in an effort to obtain the maximum amount of folded hexamer. Ultimately, the folded hexamer was purified by SEC and concentrated using Microcon YM-3 centrifugal filter devices.

Catalytic Activity Measurements. The catalytic activity of each 4OT analogue was assayed using the substrate 2-HM according to previously reported protocols (*22*). Briefly, this was accomplished by monitoring the change in absorbance at 232 nm, corresponding to the rate of product formation. Data were collected in 1 s intervals over a 5 s time period, and catalytic rates were determined in absorbance units per second by linear least-squares analysis of the raw data. All activity measurements were recorded in 20 mM phosphate buffer (pH 7.0). In these activity assays, the final concentration of the enzyme was 1−50 nM and the final concentration of the substrate was 20−100 μM.

GuHCl-Induced Equilibrium Unfolding Experiments. In experiments that were designed to evaluate the reversibility of the 4OT(N), (OI2)4OT, and (OI7)4OT unfolding reactions, folded and unfolded stock solutions of each analogue were prepared from a concentrated solution of each SEC-purified hexamer. The folded stock solutions of each analogue were prepared in a buffer that contained 50 mM Tris buffer (pH 7.0) and 0.5 M NaCl, and the unfolded stock solutions of each analogue were prepared in a buffer that contained 50 mM Tris buffer (pH 7.0), 0.5 M NaCl, and denaturing concentrations of GuHCl [i.e., 2 M GuHCl in the case of (OI2)4OT and (OI7)4OT and 3 M GuHCl in the case of 4OT(N)]. Catalytic activity measurements were utilized to confirm that each anaologue was in fact folded and unfolded in the appropriate stock solution. Ultimately, these folded and unfolded stock solutions of each analogue were then diluted into a series of buffers containing 20 mM phosphate buffer (pH 7.0) and concentrations of GuHCl that varied from 0 to 4 M so equilibrium unfolding and refolding curves, respectively, could be recorded for each analogue. This was accomplished by monitoring the catalytic activity of each solution after various equilibration times. We note that the unfolding and refolding curves for 4OT(N) and (OI2)4OT were coincident after an equilibration time of ~12 h, and the unfolding and refolding curves for (OI7)4OT were coincident after an equilibration time of 5 days. The long equilibration time for the (OI7)4OT experiment was specifically required for the solutions in the transition region of this analogue's unfolding curve to reach equilibrium.

The enzyme solutions used to generate the GuHCl-induced equilibrium unfolding curves for each analogue in this work were prepared by mixing two different stock solutions. One stock solution contained folded enzyme in 50 mM Tris buffer (pH 7.0) containing 0.5 M NaCl, and the other stock solution contained unfolded enzyme in 50 mM Tris buffer (pH 7.0) containing 0.5 M NaCl and 6 M GuHCl. Both of these stock solutions were prepared by 10-fold dilution of a folded 4OT hexamer solution that had been purified by SEC and concentrated using Microcon YM-3 centrifugal filter devices. The folded and unfolded stock solutions were mixed in appropriate ratios to generate a series of equimolar enzyme solutions with GuHCl concentrations ranging from 0.0 to 5.0 M. All the protein solutions used in the equilibrium unfolding experiments on 4OT(N) and (OI2)4OT were equilibrated overnight at room temperature before analysis. All the protein solutions used in the equilibrium unfolding experiments on (OI7)4OT were equilibrated for 5 days at room temperature before analysis.

The equilibrated solutions used to generate the unfolding curves in this work were analyzed by RP-HPLC to determine the amount of hydrolyzed material in our experiments. Unfortunately, the small amount of protein in each individual solution was not enough to be detected in our RP-HPLC assay. In an attempt to gauge the relative amounts of hydrolyzed products in our experiments with (OI2)4OT and (OI7)4OT, we combined the solutions used to generate each analogue's unfolding curves, and subjected these pooled samples to RP-HPLC analysis. A comparison of the peak areas for the full-length polypeptide chain and the truncated hydrolysis product revealed that ~40% of the (OI7)4OT construct and ~50% of the (OI2)4OT construct had hydrolyzed. We hypothesized that the large majority of the hydrolyzed material in each pooled sample had come from equilibrium unfolding solutions in the unfolded baseline of the denaturation curve. This was confirmed in two experiments. In one experiment, (OI7)4OT solutions used to establish the folded baseline, the transition region, and the unfolded baseline were combined and analyzed by RP-HPLC. The amount of hydrolysis we detected in our RP-HPLC assay of these pooled samples was 5, 27, and 70% for the pooled solutions from the folded baseline, the transition region, and the unfolded baseline, respectively. In

a second experiment, we prepared large volumes of 30 μM solutions of (OI2)4OT in 50 mM Tris buffer (pH 7.0) containing 0.5 M NaCl and a GuHCl concentration that corresponded to concentrations in the folded baseline, transition region, and unfolded baseline of the (OI2)4OT denaturation curve (0.5, 0.75, and 1.35 M GuHCl, respectively). After equilibration, RP-HPLC analysis of these solutions indicated that the amount of hydrolyzed material in each solution was 17, 34, and 79%, respectively.

In this work, GuHCl-induced equilibrium unfolding curves were obtained on 4OT analogues at pH 7.0 using catalytic activity and far-UV CD as structural probes of the unfolding reaction. We have previously shown that catalytic activity is a useful structural probe for monitoring the equilibrium unfolding properties of this enzyme system (*22*, *25*). This is the case because the catalytic reaction is essentially diffusion-limited and the equilibration times for the 4OT equilibrium unfolding−refolding reactions are relatively long (see above). The concentration of enzyme was 30 μM (based on monomer) for each analogue. Experiments were carried out at pH 7.0 to minimize ester bond hydrolysis. Raw data from catalytic activity measurements and far-UV CD were normalized by converting the raw signal to the apparent fraction of unfolded enzyme (F_{app}) according to eq 1 (*23*):

$$F_{app} = \frac{S - S_F}{S_U - S_F} \quad (1)$$

where S is the catalytic rate or the far-UV CD signal at either 222 or 230 nm at a given GuHCl concentration and S_F and S_U are the signals of the folded and unfolded forms of the enzyme, respectively, at each GuHCl concentration. In our experiments, S was linearly dependent on the GuHCl concentration in both the folded and unfolded baselines, so linear extrapolations from these baselines were used to estimate S_F and S_U values in the transition region.

In cases where the unfolding transitions monitored by catalytic activity and far-UV CD were coincident, the normalized activity and far-UV CD data were fit to the following two-state (folded and unfolded) model (*22*):

$$H \leftrightarrow 6M \quad (2)$$

where H and M represent the folded hexamer and unfolded monomer, respectively. The equilibrium constant for the unfolding reaction in eq 2 can be written in the following form:

$$K_{eq} = \frac{6[M]^6}{[P_{tot}]_M - [M]} \quad (3)$$

where $[P_{tot}]_M$ is the total protein concentration in terms of the monomer and [M] is the concentration of the unfolded monomer. If the apparent fraction of unfolded enzyme, F_{app}, is defined as $[M]/[P_{tot}]_M$, the equilibrium constant in eq 3 can be rewritten in the following form:

$$K_{app} = \frac{6F_{app}{}^6[P_{tot}]_M{}^5}{1 - F_{app}} \quad (4)$$

where K_{app} is the apparent equilibrium constant at each GuHCl concentration. For a two-state unfolding process and at moderate to high denaturant concentrations, the apparent free energy of unfolding (ΔG_{H_2O}) is linearly dependent on the molar concentration of the denaturant according to eq 5 (*23*, *24*):

$$\Delta G_{app} = \Delta G_{H_2O} + m_g[\text{denaturant}] \quad (5)$$

where ΔG_{app} is the apparent free energy of unfolding at a particular denaturant concentration and at standard state (1 M hexamer), m_g is the constant of proportionality ($\delta\Delta G_{app}/\delta$[GuHCl]), and ΔG_{H_2O} is the free energy change of unfolding in the absence of denaturant.

In equilibrium studies of the chemical denaturant-induced unfolding of proteins, thermodynamic parameters are typically obtained by using a nonlinear least-squares analysis to fit the dependence of F_{app} upon the chemical denaturant concentration. This global fitting of the data requires an expression for F_{app} in terms of denaturant concentration, $[P_{tot}]_M$, ΔG_{H_2O}, and m_g. Such an expression for F_{app} is not easily derived in the case of our H ↔ 6M model due to the high order of eq 4. This ultimately precludes the use of standard nonlinear least-squares analysis programs based on the Marquardt−Levenberg algorithm in fitting the data in our denaturation curves to these models. Therefore, in our two-state analyses of the equilibrium unfolding curves in this work, we extracted ΔG_{H-6M} and m_{H-6M} values from the data by using eqs 4 and 5 and the expression $\Delta G_{app} = -RT\ln(K_{app})$ to convert F_{app} values in the transition region of each denaturation curve to ΔG_{app} values. In these calculations, the points in the transition region were defined as all points in which F_{app} values were between 0.05 and 0.95. These ΔG_{app} values were then used to generate plots of ΔG_{app} versus GuHCl concentration. Ultimately, a linear least-squares analysis of these plots of the data yielded m_{H-6M} values and extrapolated ΔG_{H-6M} values for each analogue.

In cases where the catalytic activity and far-UV CD unfolding transitions for a given analogue were not coincident, the normalized activity and far-UV CD data were fit to the following three-state unfolding model:

$$H \leftrightarrow 3D \leftrightarrow 6M \quad (6)$$

where H and M represent the folded hexamer and unfolded monomer, respectively, and D represents a partially folded dimeric intermediate that we have previously identified in the GuHCl-induced equilibrium unfolding of 4OT at pH ≤7.4 (*22*, *25*). According to the above three-state model, the total fraction of species present in solution at any given GuHCl concentration in our unfolding curves can be expressed according to eq 7:

$$1 = F_H + F_D + F_M \quad (7)$$

where F_H, F_D, and F_M represent the fraction of hexamer, dimer, and monomer, respectively. Since only the native hexamer is catalytically active, F_H can be determined from eq 8:

$$F_H = 1 - F_{app-act} \quad (8)$$

where $F_{app-act}$ is the apparent fraction of unfolded enzyme as determined by catalytic activity. The far-UV CD signal at each GuHCl concentration is comprised of the total contributions from the folded hexamer, folded dimer, and

Table 1: Calculated Energies and Bond Angles of Amide and Ester Bonds in Model Dipeptides Used in 4OT Analogues[a]

dipeptide	C(O)−N−C_α or C(O)−O−C_α bond angle (deg)[b]	C_α−C═O bond angle (deg)[b]	C_α−C(O)−N or C_α−C(O)−O bond angle (deg)[b]	N−C═O or O−C═O bond angle (deg)[b]	$\Delta E_{cis-trans}$ (kcal/mol)[c]	$\Delta E^{\ddagger}_{cis-trans}$ (kcal/mol)[d]
Pro-Ile	122.3	122.0	116.6	121.5	2.2	11.9
Pro-OIle	117.7	122.9	109.3	127.8	6.3	3.4
His-Ile	121.1	124.1	117.4	118.5	5.6	11.8
His-OIle	117.6	123.8	109.2	126.9	5.3	4.8

[a] Calculations were performed using Macromodel. [b] Bond angles were determined from structures that had been minimized using an mm2 force field. [c] Total energy of the *cis* conformation relative to the total energy of the *trans* conformation. [d] Energy barrier to rotation from the *cis* to the *trans* conformation.

unfolded monomer according to eq 9:

$$F_{CD} = a(F_H) + b(F_D) + c(F_M) \quad (9)$$

where F_{CD} is the apparent fraction of folded enzyme as determined by the far-UV CD signal at 222 nm and *a*, *b*, and *c* are constants that represent the weighted contributions of each species to the total far-UV CD signal at 222 nm. At each GuHCl concentration, F_{CD} can be calculated as $1 - F_{app-CD}$, where F_{app-CD} is the apparent fraction of unfolded enzyme as determined by the far-UV CD signal at 222 nm. Since F_{CD} represents the normalized CD data, then a folded 4OT hexamer contributes the maximum possible CD signal, so $a = 1$ in eq 9. Similarly, an unfolded monomer contributes the minimum possible CD signal, so $c = 0$ in eq 9. On the basis of the results of our earlier studies (*25*), the far-UV CD signal of the partially folded 4OT dimer is approximately 80% of the folded hexamer signal at 222 nm, so *b* in eq 9 can be assigned a value of 0.8. Using these assignments for *a*, *b*, and *c*, along with eqs 8 and 9, F_D can be calculated at every GuHCl concentration according to eq 10:

$$F_D = (F_{app-act} - F_{app-cd})/0.8 \quad (10)$$

The equilibrium constants for the unfolding reaction in eq 6 can be written as follows:

$$K_{H-3D} = \frac{[D]^3}{[H]} \quad (11)$$

$$K_{3D-6M} = \frac{[M]^6}{[D]^3} \quad (12)$$

where [H], [D], and [M] are the concentrations of the hexamer, dimer, and monomer, respectively. In our three-state analyses, eqs 7−10 were used to evaluate F_H, F_D, and F_M at each GuHCl concentration in our denaturation curves. The resulting values for F_H, F_D, and F_M were then multiplied by the total protein concentration ($[P_{tot}]$) to obtain values for [H], [D], and [M], respectively. The values for [H], [D], and [M] were then used in combination with eqs 11 and 12 to calculate two apparent equilibrium constants ($K_{appH-3D}$ and $K_{app3D-6M}$) at each GuHCl concentration. The $K_{appH-3D}$ and $K_{app3D-6M}$ values we calculated at each GuHCl concentration in the unfolding transition were converted to $\Delta G_{appH-3D}$ and $\Delta G_{app3D-6M}$, respectively, using the expression $\Delta G_{app} = -RT \ln(K_{app})$. These values were used to generate plots of $\Delta G_{appH-3D}$ and $\Delta G_{app3D-6M}$ versus GuHCl concentration, and a linear least-squares analysis of the data from each plot yielded values for m_{H-3D}, m_{3D-6M}, ΔG_{H-3D}, and ΔG_{3D-6M}.

Theoretical Calculations. Solvent-accessible surface area (SAS) calculations were performed using the X-ray crystallographic data that are available for the wild-type 4OT hexamer (*26*) to determine the extant to which each mutation site was buried upon folding (*27*, *28*). SAS measurements were calculated for each amino acid residue in all six subunits of the wild-type hexamer using the ACCESS program and a 1.4 Å probe. The SAS of Ile2 and of Ile7 was calculated in each subunit, and the values obtained for each residue in all six subunits were averaged. The average SAS values and standard deviations obtained for Ile2 and Ile7 were 3.9 ± 1.6 and 1.1 ± 1.6 Å^2, respectively. These values were compared to the total SAS of corresponding residues in an extended polypeptide chain, as calculated by Creamer and co-workers (*29*). Ultimately, the %ΔSAS was determined for residues 2 and 7 in the wild-type structure, the sites of the amide-to-ester bond mutations in this study. On the basis of these calculations, Ile2 and Ile7 are 98 and 99% buried, respectively, upon folding.

As part of this work, we also performed a series of molecular modeling experiments to compare the physical properties of the ester bond mutations in the 4OT analogues studied here to the physical properties of the corresponding native amide bond at each mutation site. Using the computer modeling program, Macromodel, dipeptides that contained the native amide bonds (i.e., Pro−Ile and His−Ile) and the mutated ester bonds (i.e., Pro−OIle and His−OIle) were constructed, and the structures were minimized in the *trans* conformation using an mm2 force field and fixed bond lengths. The C−C, C(O)−O, C(O)−N, C−O, and C−N bond lengths in the peptide backbone were set to 1.53, 1.37, 1.39, 1.41, and 1.47 Å, respectively. The resulting bond angles and total energies that were calculated for each dipeptide and the corresponding ester bond mutant are summarized in Table 1.

RESULTS AND DISCUSSION

Amide-to-Ester Bond Mutation. The ester bond is an attractive amide bond isostere for modulating the hydrogen bonding characteristics of a protein's polypeptide backbone. Our calculations on model dipeptides indicate that the ester bonds in (OI2)4OT and (OI7)4OT are very similar to the amide bonds they replace in that they favor the *trans* configuration, they are planar, and they have bond angles similar to those of an amide bond (see Table 1). One difference between the ester bonds and the amide bonds in our 4OT analogues is that the energy barrier to *cis*−*trans* rotation is substantially larger for the amide bonds. However, these differences in the energy barrier to *cis*−*trans* rotation

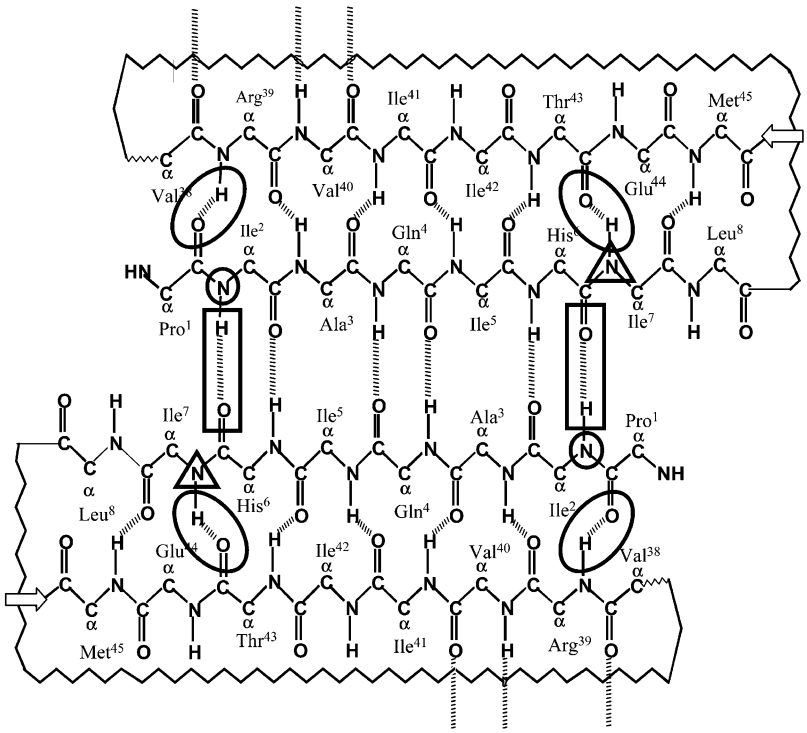

FIGURE 1: Schematic representation of the putative backbone−backbone hydrogen bonds in one of the intersubunit β-sheet regions of 4OT's native three-dimensional structure. The amide-to-ester bond mutation sites in (OI2)4OT and (OI7)4OT are highlighted with circles and triangles, respectively. The hydrogen bond deletion that is common to both analogues is highlighted with a rectangle. The hydrogen bond deletion that is unique to each analogue is highlighted with an oval. There are two additional intersubunit β-sheet regions in the 4OT hexamer that are identical to the one shown above. Therefore, in each analogue, there are a total of six amide-to-ester mutations per hexamer (i.e., one mutation per subunit).

will not impact the thermodynamic results presented below, as they were obtained under equilibrium conditions.

An important difference between the ester bonds and the amide bonds in our 4OT analogues is that the hydrogen bonding characteristics of the ester bonds in (OI2)4OT and (OI7)4OT are very different from those of the amide bonds that they replace. In contrast to the amide bond, the ester bond lacks a hydrogen bond donor (i.e., there is an O atom in place of an NH group). It has also been noted that the pK_a of an ester bond carbonyl is lower than that of an amide bond carbonyl, which suggests that it is a poorer hydrogen bond acceptor than an amide carbonyl (*30*). Thus, the ester bond mutations in (OI2)4OT and (OI7)4OT are each expected to effectively delete a pair of backbone−backbone hydrogen bonds per monomer in 4OT's native three-dimensional structure (see Figure 1).

Structural Characterization of Folded 4OT Analogues. The purified synthetic products obtained from our syntheses of 4OT(N), (OI2)4OT, and (OI7)4OT were each subjected to a folding protocol and then analyzed by SEC (Figure 2). A major peak at 12 min was detected in the SEC chromatogram of each analogue. The retention time of these peaks (12 min) is consistent with the retention time of the native 4OT hexamer. ESI-MS analysis of the material that eluted under each 12 min peak in Figure 2 also confirmed that the material eluting in each peak was the full-length polypeptide chain of each analogue. A second peak at 14 min was also observed in the SEC chromatograms of each analogue. ESI-MS mass spectra collected on the material that eluted in these 14 min peaks indicated the presence of full-length material as well as minor amounts of truncated impurities that evidently remained after the synthesis and purification of each

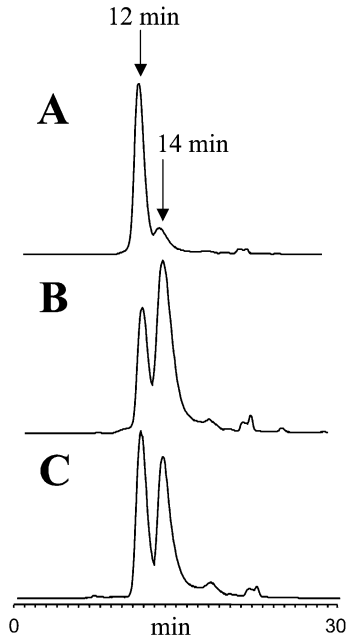

FIGURE 2: SEC elution profiles obtained for (A) 4OT(N), (B) (OI2)4OT, and (C) (OI7)4OT.

analogue. We note that the impurities we detected in our mass spectrometry analyses did not include any of the byproducts expected from hydrolysis of the ester bonds in our constructs. We also note that the purities of our synthetic analogues were comparable to each other as judged by RP-HPLC and ESI mass spectrometry.

The material that eluted in the 12 min peaks in our SEC chromatograms was collected and further characterized by

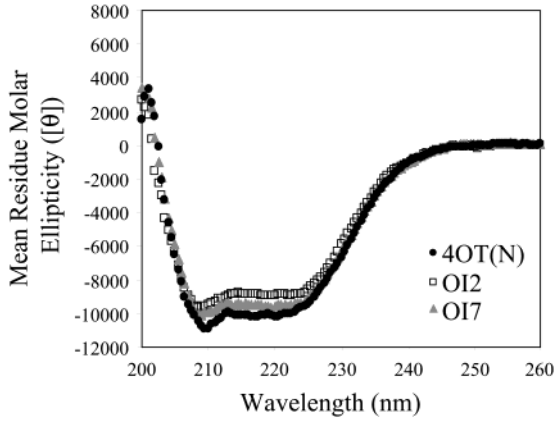

FIGURE 3: Far-UV CD spectrum of material isolated from the 12 min peaks in the SEC elution profiles of 4OT(N), (OI2)4OT, and (OI7)4OT.

Table 2: Catalytic Activity Parameters of 4OT Analogues with 2-HM at pH 7.0 and 25 °C

analogue	k_{cat} (s^{-1})	K_M (μM)	k_{cat}/K_M (s^{-1} M^{-1})
4OT(N)	1.6×10^3	93	1.9×10^7
OI2	0.2×10^3	96	2.5×10^6
OI7	1.4×10^3	68	2.1×10^7

far-UV CD spectroscopy. Figure 3 shows the far-UV CD spectra recorded for material isolated in the 12 min SEC peaks of 4OT(N), (OI2)4OT, and (OI7)4OT. The three spectra that we recorded were nearly identical, and each spectrum was essentially the same as a far-UV CD spectrum previously recorded on a preparation of the wild-type enzyme obtained by recombinant DNA methods (*13*). The material that eluted in the 12 min peaks in our SEC chromatograms of 4OT(N), (OI2)4OT, and (OI7)4OT was also assayed for catalytic activity using the substrate 2-HM. The catalytic properties of (OI2)4OT and (OI7)4OT constitute a sensitive structural probe of the folded, three-dimensional structure of these analogues as the ester bond mutation in each analogue is located at a position in the enzyme's three-dimensional structure that is very close to the active site. Any significant structural perturbations caused by the amide-to-ester bond mutations in these analogues are likely to have a deleterious effect on the enzyme's catalytic efficiency. The kinetic parameters, k_{cat} and K_M, obtained for each analogue are summarized in Table 2.

We have previously shown that the catalytic properties of 4OT(N) are essentially identical to those of the wild-type enzyme obtained by recombinant DNA techniques (*20*). As expected, the k_{cat} and K_M values we determined for the 4OT(N) preparation used in this work were essentially identical to those of the wild-type enzyme. The catalytic parameters we determined for (OI7)4OT were also very similar to those determined for the wild-type enzyme. The catalytic properties of (OI2)4OT were only slightly altered from that of the wild-type enzyme. In particular, the k_{cat} value calculated for this analogue was approximately 8-fold lower than the value reported for the wild-type enzyme. This drop in k_{cat} may be due to a small structural perturbation in the active site of the (OI2)4OT analogue. This change in the active site is most likely related to a slight repositioning of the catalytic base, Pro1.

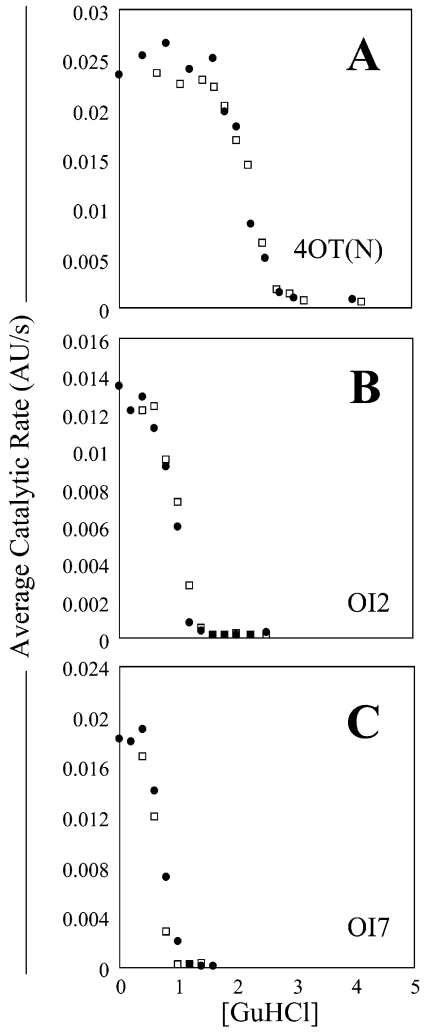

FIGURE 4: GuHCl-induced denaturation curves (●) and renaturation curves (□) obtained for (A) 4OT(N), (B) (OI2)4OT, and (C) (OI7)4OT as monitored by catalytic activity with 2-HM at pH 7.0 and 25 °C. Measurements were obtained in 50 mM Tris buffer containing 0.5 M NaCl, and the enzyme concentration was 30 μM for each analogue.

The 12 to 14 min peak area ratio was different in each SEC elution profile shown in Figure 1. We attribute the different peak area ratios to differences in the folding yields of our synthetic analogues and not to the presence of different equilibria. Evidence supporting this conclusion comes from the fact that when material isolated exclusively from each 12 min peak is collected, equilibrated, and re-injected onto the size-exclusion column, only a single peak at 12 min is observed (data not shown). CD analysis and catalytic activity measurements on material isolated in the 14 min peaks of the SEC elution profiles in Figure 1 also show that the material in these 14 min peaks is largely unfolded and displays no detectable enzymatic properties.

Thermodynamic Analysis of Folded 4OT Analogues. The reversibility of the GuHCl-induced equilibrium unfolding of each 4OT analogue in this study was determined by examining the unfolding and refolding curves generated using catalytic activity measurements. The unfolding curves we generated for 4OT(N), (OI2)4OT, and (OI7)4OT were coincident with the refolding curves generated for each analogue (see Figure 4). In similar experiments, we have

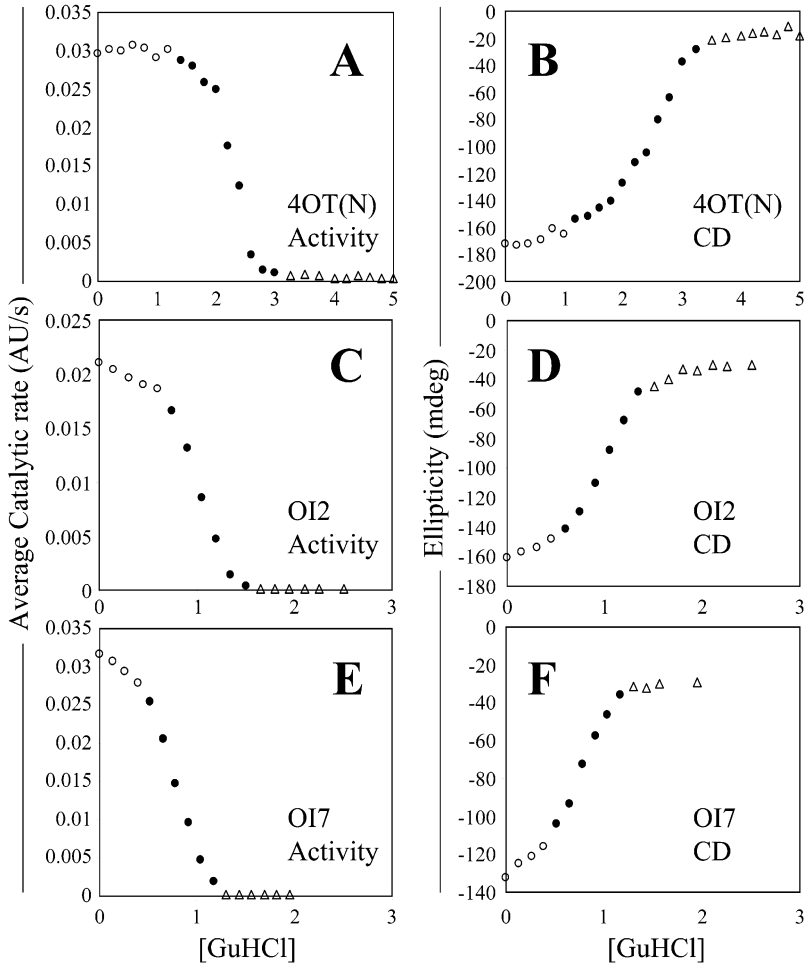

FIGURE 5: GuHCl-induced equilibrium unfolding curves for 4OT(N), (OI2)4OT, and (OI7)4OT as monitored by far-UV CD at 222 nm and catalytic activity with 2-HM at pH 7.0 and 25 °C. The points represent the raw data that were used to construct the normalized curves in Figure 6. The data points used to establish the pre- and post-transition baselines in each case are represented as empty circles and empty triangles, repsectively. Measurements were obtained in 50 mM Tris buffer containing 0.5 M NaCl, and the enzyme concentration was 30 μM for each analogue.

also established that the GuHCl-induced equilibrium unfolding transition of wild-type 4OT is reversible (*20*).

The GuHCl-induced equilibrium unfolding transitions of the (OI2)4OT, (OI7)4OT, and 4OT(N) constructs in this work were monitored at pH 7.0 by far-UV CD and by catalytic activity measurements. Typical raw data that we obtained in these experiments are shown in Figure 5, and the normalized unfolding curves we obtained for each protein construct are shown in Figure 6. In the case of 4OT(N), the catalytic activity transition midpoint of 1.9 M GuHCl preceded the far-UV CD transition midpoint of 2.5 M GuHCl. The catalytic activity transition was also significantly more cooperative than the far-UV CD transition. These results with 4OT(N) are consistent with the formation of a partially folded, catalytically inactive folding intermediate, and they are similar to results previously obtained with the wild-type enzyme (*22*, *25*).

Using a preparation of the enzyme obtained by recombinant DNA methods, we have previously established that a partially folded and catalytically inactive dimeric intermediate state of 4OT is populated in solution at pH $\leq$7.4. Thus, in our analysis of the normalized equilibrium unfolding data for 4OT(N) shown in Figure 6A, the data were fit to a three-state model in which we assumed that the only species populated at equilibrium were the folded hexamer, a partially folded dimer, and the unfolded monomer. The results of our three-state analysis of 4OT(N)'s equilibrium unfolding reaction are shown in Figure 7. The thermodynamic parameters (i.e., m_{H-3D}, m_{3D-6M}, ΔG_{H-3D}, and ΔG_{3D-6M}) obtained from our linear least-squares analysis of the data and from a similar analysis of two additional data sets are summarized in Table 3. Summarized in Table 4 are the overall ΔG_{H-6M} and m_{H-6M} values we obtained for the GuHCl-induced unfolding of a 4OT(N) hexamer to six unfolded monomers. These ΔG_{H-6M} and m_{H-6M} values are essentially identical to those of the wild-type enzyme obtained by recombinant DNA methods (Table 4).

In contrast to our results with 4OT(N), the far-UV CD and catalytic activity unfolding transitions we measured for the two ester bond-containing analogues, (OI2)4OT and (OI7)4OT, were nearly identical (i.e., displayed the same cooperativity and had similar transition midpoints) (see panels B and C of Figure 6). The coincidence of the far-UV CD and catalytic activity unfolding transitions for (OI2)4OT and (OI7)4OT suggests that the GuHCl-induced equilibrium unfolding behavior of these analogues should be modeled well by a two-state process involving a folded hexamer and an unfolded monomer. Shown in Figure 8 are the results of

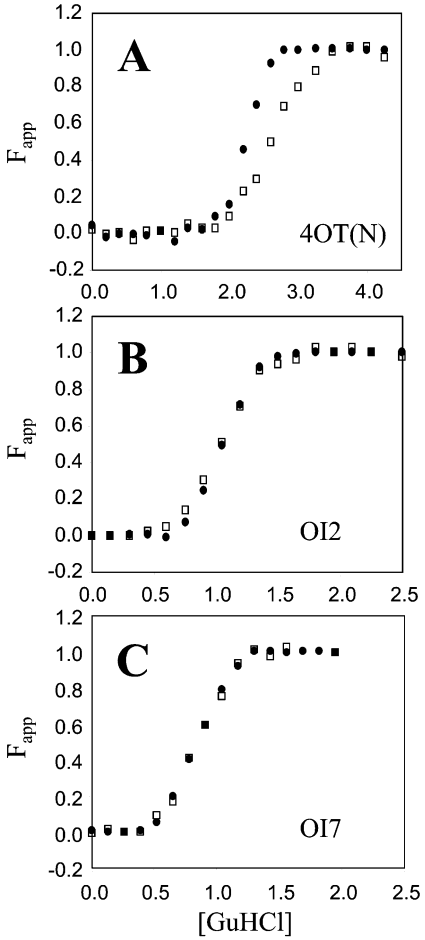

FIGURE 6: Normalized data from the GuHCl-induced equilibrium unfolding of (A) 4OT(N), (B) (OI2)4OT, and (C) (OI7)4OT as monitored by far-UV CD (□) and catalytic activity with 2-HM (●) at pH 7.0 and 25 °C. Measurements were obtained in 50 mM Tris buffer containing 0.5 M NaCl, and the enzyme concentration was 30 μM for each analogue.

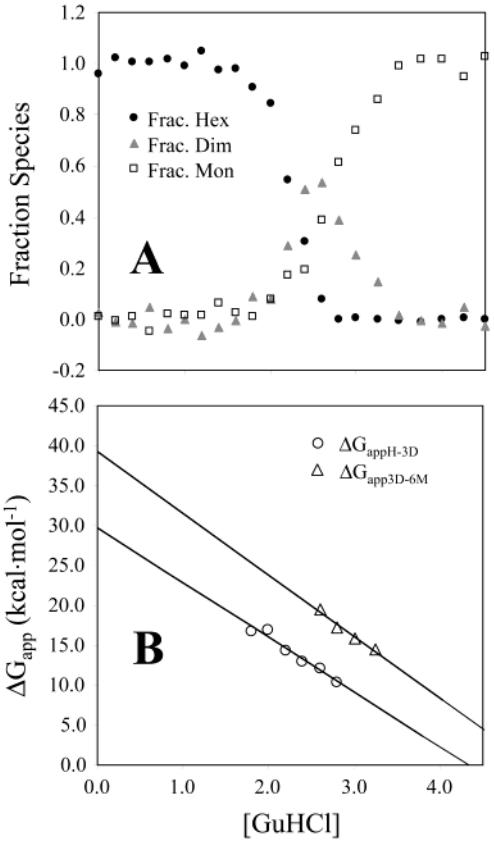

FIGURE 7: Three-state analysis of the GuHCl-induced equilibrium unfolding of 4OT(N) at pH 7.0 and 25 °C. (A) The fraction of hexamer (●), the fraction of partially folded dimer (▲), and the fraction of unfolded monomer (□) are plotted as a function of GuHCl concentration. (B) Best fit of the data in the catalytic activity and far UV-CD unfolding transition regions to a three-state model involving a folded hexamer, a partially folded dimer, and an unfolded monomer.

our two-state analysis of representative equilibrium unfolding data obtained for (OI2)4OT and (OI7)4OT. The thermodynamic parameters obtained from these analyses are summarized in Table 4. The ΔG_{H-6M} and m_{H-6M} values calculated for each analogue were almost within one standard deviation of each other, indicating that the measured values are essentially the same considering the error of the experiment.

The equilibrium unfolding behavior we observed for (OI2)4OT and (OI7)4OT suggests that the amide-to-ester bond mutations in these analogues apparently destabilize the partially folded dimeric species populated in the equilibrium unfolding reaction of the wild-type enzyme to the extant that it was not significantly populated in the equilibrium unfolding reactions of (OI2)4OT or (OI7)4OT. This is not surprising as one of the hydrogen bonds that is effectively deleted in both the (OI2)4OT and (OI7)4OT analogues lies at a major subunit interface in the partially folded dimer (see Figure 1).

One potential complication associated with using ester bond-containing protein analogues in protein folding studies is that the ester bond is susceptible to hydrolysis. As noted above, the ester bonds in (OI2)4OT and (OI7)4OT were not hydrolyzed over the time course of the folding protocol. We also found that the ester bonds in these two analogues were not subject to hydrolysis when they were folded in buffer and stored for extended periods of time (up to 24 h). However, we did find that the ester bonds in (OI2)4OT and (OI7)4OT were both susceptible to hydrolysis when the analogues were denatured in GuHCl. The amount of hydrolysis in the solutions used to generate the (OI2)4OT and (OI7)4OT denaturation curves in this work was quantified by RP-HPLC analysis. The results of our RP-HPLC analyses showed that the greatest amount of hydrolysis occurred in the (OI2)4OT and (OI7)4OT solutions used to generate the post-transition baselines of these analogues' denaturation curves where it had little impact on our calculations of ΔG_{H-6M} and m_{H-6M}. The shape and position of the pre-transition and transition regions of our denaturation curves had the largest impact on our calculations of ΔG_{H-6M} and m_{H-6M}. In these regions, the amount of hydrolysis was not

Table 3: Three-State Thermodynamic Analysis of the GuHCl-Induced Equilibrium Unfolding of 4OT(N) at pH 7.0 and 25 °C

trial	ΔG_{H-3D} (kcal/mol)	m_{H-3D} (kcal mol^{-1} M^{-1})	ΔG_{3D-6M} (kcal/mol)	m_{3D-6M} (kcal/mol)
1	30.9 ± 0.7[a]	7.0 ± 0.3[a]	43.3 ± 3.5[a]	9.3 ± 1.2[a]
2	29.2 ± 2.4[a]	6.6 ± 1.1[a]	39.3 ± 2.4[a]	7.7 ± 0.8[a]
3	26.1 ± 1.0[a]	5.3 ± 0.5[a]	40.2 ± 6.1[a]	8.4 ± 2.1[a]
average	28.7 ± 2.5[b]	6.3 ± 0.9[b]	40.9 ± 2.0[b]	8.5 ± 0.8[b]

[a] Values are reported with a standard error from linear least-squares analysis. [b] Average values are reported with a standard deviation.

Table 4: Thermodynamic Analysis of 4OT Analogues after GuHCl-Induced Equilibrium Unfolding at pH 7.0 and 25 °C

analogue	ΔG_{H-6M} (kcal/mol)[a]	m_{H-6M} (kcal mol^{-1} M^{-1})[a]	$\Delta\Delta G$ (kcal/mol)
wild-type 4OT	70.4 ± 3.6[b]	14.9 ± 1.3[b]	–
4OT(N)	69.6 ± 3.3[b]	14.8 ± 1.2[b]	–
OI2	47.7 ± 2.5[c]	15.0 ± 2.2[c]	21.9
OI7	45.0 ± 2.5[c]	15.3 ± 1.6[c]	24.6

[a] Values obtained for wild-type 4OT were calculated from data acquired at pH 7.4 in ref *22*, represent the average of three separate experiments, and are reported with a standard deviation. Values obtained for 4OT(N) are the average values and standard deviations calculated from the data in Table 3. Values obtained for OI2 and OI7 are the average values and standard deviations obtained from one CD denaturation curve and at least two different activity denaturation curves. [b] Values were calculated using an apparent three-state equilibrium unfolding model involving a folded hexamer, an unfolded monomer, and a partially folded, dimeric intermediate. [c] Values were calculated using an apparent two-state equilibrium unfolding model involving only a folded hexamer and an unfolded monomer.

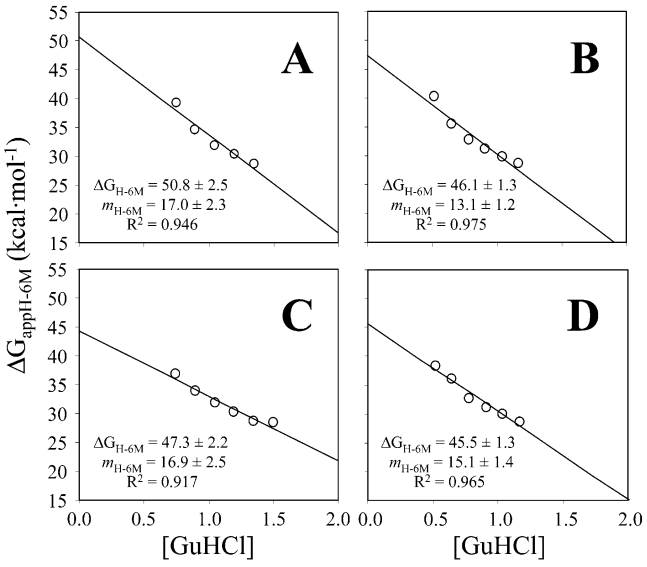

FIGURE 8: Two-state analysis of the equilibrium unfolding data obtained for (OI2)4OT and (OI7)4OT at pH 7.0 and 25 °C. Shown in panels A and B are the best fits of the (OI2)4OT data in the catalytic activity and the far-UV CD unfolding transition regions, respectively, to a two-state model involving a folded hexamer and an unfolded monomer. Shown in panels C and D are the best fits of the (OI7)4OT data in the catalytic activity and the far UV-CD unfolding transition regions, respectively, to a two-state model involving a folded hexamer and an unfolded monomer.

large enough to have a significant impact on our calculations of ΔG_{H-6M} and m_{H-6M} (see below). It is also noteworthy that the (OI2)4OT and (OI7)4OT constructs were hydrolyzed to approximately the same extant in our experiments despite the different equilibration times (12 h and 5 days, respectively) required for these analogues. These observations are consistent with the ester bond in these analogues being susceptible to hydrolysis in only their denatured states.

In earlier studies, we have shown that the polypeptide product generated by hydrolysis of the ester bond in (OI2)4OT does not fold into a hexamer or adopt any significant secondary structure (*13*). Thus, the hydrolyzed material in our equilibrium unfolding experiments is not expected to contribute to the catalytic activity measurements in panels B and C of Figure 6. The presence of unfolded the 4OT monomer has the potential to reduce the CD signal in our unfolding experiments. However, we note that the significant amounts of hydrolyzed product (i.e., >30%) are only present at high GuHCl concentrations where the protein is largely unfolded and the CD signal of the full-length material is already weak.

The presence of hydrolyzed material in our equilibrium unfolding experiments with (OI2)4OT and (OI7)4OT could potentially affect the shape and position of each analogue's unfolding curve. However, we estimate that these effects are small. For example, the hydrolysis reaction in our unfolding experiments is expected to reduce the concentration of full-length and folding competent polypeptide chains. Since 4OT is a hexamer, its stability is concentration-dependent. Therefore, a reduction in protein concentration would be expected to shift the transition midpoint of our unfolding curve to a lower GuHCl concentration and lead to the calculation of a smaller ΔG_{H-6M} value. However, we note that the amount of hydrolyzed material detected in the solutions used to define the transition midpoints of our curves (i.e., ∼30%) would only be expected to shift the midpoint by ∼0.1 M. This potential error is roughly equivalent to the error associated with determining the GuHCl concentration at our transition midpoints. Moreover, a 0.1 M shift of the denaturation curves in Figure 6 would only alter our ΔG value determinations by less than 5%. This is evidenced by the fact that the *y*-intercepts of the lines plotted in Figure 8 change by less than 5% when the *x*-coordinates of the data points in each graph are shifted 0.1 M unit.

The presence of hydrolyzed material in our unfolding experiments also has the potential to impact the shape of our unfolding curves. If the increasing amounts of hydrolyzed product in the sample solutions used to define the transition region of our (OI2)4OT and (OI7)4OT unfolding curves were significant, then our ΔG_{app} versus GuHCl concentration plots would be nonlinear. This would lead to the calculation of erroneous ΔG_{H_2O} and m_g values. We note that our plots of ΔG_{app} versus GuHCl concentration were essentially linear (see Figure 8) and that the *m* values we determined for (OI2)4OT and (OI7)4OT are essentially identical to the *m* value we determined for 4OT(N). Taken together, these results suggest that the hydrolyzed material present in our equilibrium unfolding experiments with (OI2)4OT and (OI7)4OT did not significantly impact our ability to calculate reliable ΔG_{H-6M} and m_{H-6M} values for unfolding reactions of these analogues.

Implications for Backbone−Backbone Hydrogen Bonding in Proteins. The results of our thermodynamic studies indicate that the ester bond mutations in (OI2)4OT and (OI7)4OT decreased the overall thermodynamic stability of the 4OT hexamer. Unfortunately, it is difficult to ascertain from our thermodynamic data the exact energetic contribution of the 12 hydrogen bond deletions (two per monomer) in (OI2)4OT and the 12 hydrogen bond deletions (two per monomer) in (OI7)4OT. While the 12 native backbone−backbone hydrogen bond deletions in each analogue certainly contribute to the net destabilization measured for each analogue, there are likely additional effects that could potentially contribute to the net destabilization measured for each analogue. The ester bond mutation could potentially alter the solvation properties of the chemically denatured polypeptide chain as well as change the structure and energy of the chemically denatured state. Unfavorable electrostatic

and van der Waals interactions between the oxygen ester and neighboring carbonyl groups could also destabilize the native structure (*1*, *15*). Replacing a backbone N atom with an O atom means that the attractive interaction with the neighboring carbonyl group becomes repulsive. This has the potential to perturb the protein's three-dimensional structure and destabilize it. However, we note that such perturbations appeared to be minimal in the case of our ester bond analogues of 4OT as evidenced from our data on the enzymatic properties of these analogues that appeared to be very similar to those of the wild-type enzyme.

The ester bonds in the (OI2)4OT and (OI7)4OT analogues are both buried in the same hydrophobic region of 4OT's three-dimensional structure; they are both in β-sheet structures with similar orientations and spacing between chains, and they are both subject to very similar chemical environments. Thus, any unfavorable electrostatic and van Waals interactions between the oxygen ester and neighboring carbonyl group in the native structure are expected to be comparable between the two analogues. Unfortunately, it is difficult to characterize the effect of each ester bond mutation on the conformational properties of the denatured state of 4OT. However, it seems reasonable to assume that effects of each ester bond in (OI2)4OT and (OI7)4OT on the conformational properties of the denatured state of 4OT will at least be similar. This is substantiated by our observation that the ester bonds in (OI2)4OT and (OI7)4OT are equally susceptible to hydrolysis under denaturing conditions. If the mutational effects of the ester bond on the native and denatured states of 4OT beyond those of the backbone−backbone hydrogen bond deletions in the native state are taken to be the same for the two analogues, then our results suggest that the backbone−backbone hydrogen bonds deleted in (OI2)4OT and (OI7)4OT make equivalent contributions to 4OT's thermodynamic stability.

The two backbone−backbone hydrogen bonds per subunit that are effectively deleted in (OI2)4OT and (OI7)4OT include one intersubunit hydrogen bond and one intrasubunit hydrogen bond (see Figure 1). The intersubunit hydrogen bond deletion is common to both analogues, and the intrasubunit hydrogen bond deletion is different in each analogue. The symmetry of the 4OT molecule is such that the two different intrasubunit hydrogen bonds deleted in (OI2)4OT and (OI7)4OT are located in positions in 4OT's three-dimensional structure that are structurally very similar. They are both positioned at the ends of the parallel β-sheet region in 4OT, and they are both equally buried in the protein structure. While the thermodynamic effects of amide-to-ester bond mutations that are buried in hydrophobic regions of a protein structure have been compared (see ref *31*), the thermodynamic effects of amide-to-ester bond mutations at structurally equivalent positions (i.e., at similar positions in an α-helix or β-sheet) have not been directly compared. In this respect, our results provide that first direct comparison of backbone−backbone hydrogen bonds located in structurally similar regions of a protein (i.e., at the ends of a β-sheet).

In conclusion, we have utilized total chemical synthesis methods to incorporate amide-to-ester bond mutations into the polypeptide backbone of 4OT to delete specific backbone−backbone hydrogen bonds within the β-sheet region of the enzyme's native three-dimensional structure. Our comparative analysis of two backbone-modified 4OT analogues, (OI2)4OT and (OI7)4OT, suggests that the different, but structurally similar, backbone−backbone hydrogen bonds in these two analogues make equivalent contributions to 4OT's thermodynamic stability.

ACKNOWLEDGMENT

We are grateful to Michael Goldsmith for his help with the dipeptide calculations and to Jeffrey Myers for his help with the SAS calculations. Acknowledgment is made to the donors of The Petroleum Research fund, administered by the ACS for partial support of this research.

REFERENCES

1. Dill, K. A. (1990) *Biochemistry 29*, 7133−7135.
2. Myers, J. K., and Oas, T. G. (1999) *Biochemistry 38*, 6761−6768.
3. Pace, C. N. (1995) *Methods Enzymol. 259*, 538−554.
4. Stickle, D. F., Pesta, L. G., Dill, K. A., and Rose, G. D. (1992) *J. Mol. Biol. 226*, 1143−1159.
5. Honig, B., and Yang, A. S. (1995) *Adv. Protein Chem. 46*, 27−58.
6. Mendel, D., Cornish, V. W., and Schultz, P. G. (1995) *Annu. Rev. Biophys. Biomol. Struct. 24*, 435−462.
7. Muir, T. W., and Kent, S. B. H. (1993) *Curr. Opin. Biotechnol. 4*, 420−427.
8. Koh, J. T., Cornish, V. W., and Schultz, P. G. (1997) *Biochemistry 36*, 11314−11322.
9. Chapman, E., Thorson, J. S., and Schultz, P. G. (1997) *J. Am. Chem. Soc. 119*, 7151−7152.
10. Lu, W., Qasim, M. A., Laskowski, M., Jr., and Kent, S. B. H. (1997) *Biochemistry 36*, 673−679.
11. Lu, W., Randal, M., Kossiakoff, A., and Kent, S. B. H. (1999) *Chem. Biol. 6*, 419−427.
12. Beligere, G. S., and Dawson, P. E. (2000) *J. Am. Chem. Soc. 122*, 12079−12082.
13. Nakhle, B. M., Silinski, P., and Fitzgerald, M. C. (2000) *J. Am. Chem. Soc. 122*, 8105−8111.
14. Wales, T. E., and Fitzgerald, M. C. (2001) *J. Am. Chem. Soc. 123*, 7709−7710.
15. Ben-Tal, N., Sitkoff, D., Topol, I. A., Yang, A. S., Burt, S. K., and Honig, B. (1997) *J. Phys. Chem. B 101*, 450−457.
16. Shi, Z., Krantz, B. A., Kallenbach, N., and Sosnick, T. R. (2002) *Biochemistry 41*, 2120−2129.
17. Krantz, B. A., Moran, L. B., Kentsis, A., and Sosnick, T. R. (2000) *Nat. Struct. Biol. 7*, 62−71.
18. Waddell, W. J. (1956) *J. Lab. Clin. Med. 48*, 311−314.
19. Pace, C. N. (1986) *Methods Enzymol. 131*, 266−279.
20. Fitzgerald, M. C., Chernushivech, I., Standing, K. G., Kent, S. B. H., and Whitman, C. P. (1995) *J. Am. Chem. Soc. 117*, 11075−11080.
21. Schnolzer, M., Alewood, P., Jones, A., Alewood, C., and Kent, S. B. H. (1992) *Int. J. Pept. Protein Res. 40*, 180−193.
22. Silinski, P., Allingham, M. J., and Fitzgerald, M. C. (2001) *Biochemistry 40*, 4493−4502.
23. Pace, C. N. (1975) *CRC Rev. Biochem.*, 1−43.
24. Santoro, M. M., and Bolen, D. W. (1992) *Biochemistry 31*, 4901−4907.
25. Silinski, P., and Fitzgerald, M. C. (2002) *Biochemistry 41*, 4480−4491.
26. Roper, D. I., Subramanya, H. S., Shingler, V., and Wigley, D. B. (1994) *J. Mol. Biol. 243*, 799−801.
27. Lee, B., and Richards, F. M. (1971) *J. Mol. Biol. 55*, 379−400.
28. Myers, J. K., Pace, C. N., and Scholtz, J. M. (1995) *Protein Sci. 4*, 2138−2148.
29. Creamer, T. P., Srinivasan, R., and Rose, G. D. (1997) *Biochemistry 36*, 2832−2835.
30. Arnett, E. M., Mitchell, E. J., and Murty, T. S. S. R. (1974) *J. Am. Chem. Soc. 96*, 3875−3891.
31. Blankenship, J. W., Balambika, R., and Dawson, P. E. (2002) *Biochemistry 41*, 15676−15684.

BI020700B